Study on transfer-free graphene synthesis process utilizing spontaneous agglomeration of catalytic Ni and Co metals

Makoto Miyoshi[1,a] Masaya Mizuno[1,2] Kazuya Banno[1,2,b] Toshiharu Kubo[1] Takashi Egawa[1] and Tetsuo Soga

[1]*Research Center for Nano Device and System, Nagoya Institute of Technology, Nagoya 466-8555, Japan*

[2]*Department of Frontier Materials, Nagoya Institute of Technology, Nagoya 466-8555, Japan*

Transfer-free graphene synthesis process utilizing metal agglomeration phenomena was investigated by using carbon films deposited on Ni or Co catalyst metals on SiO_2/Si substrates. As a result of metal agglomeration at high temperatures, multilayer graphene films appeared to be formed directly on SiO_2 films. The microscopic Raman mapping study revealed that graphene films were preferentially synthesized around areas where metal films disappeared at an early stage of agglomeration, and that they finally covered almost the whole surfaces. It was also found that the synthesized graphene films tend to have better structural qualities and lower layer numbers with the increase in the starting metal thicknesses regardless of the kinds of catalyst metals. The Raman study also showed that they had good two-dimensional uniformity in the structural quality.

---

a) Corresponding author;

E-mail address: miyoshi.makoto@nitech.ac.jp (Makoto Miyoshi)

Phone & Fax: +81-52-735-5092

b) Present affiliation: Hayashi Telempu Co., Ltd. Nagoya, Japan

1. INTRODUCTION

Due to its novel characteristics such as extremely high carrier mobility and ballistic transport properties, graphene has recently been attracting much attention as material for future high-frequency electronic devices and/or large-scale integrated circuit devices [1-4]. Since the discovery of outstanding features in this two-dimensional material, various synthesis processes have been proposed, such as the sublimation of silicon from SiC surfaces [5-8], chemical vapor deposition [9-13], and plasma-assisted vapor deposition [14-17]. Also, several kinds of catalytic metals such as Ni [9-14, 17, 18], Co [10], Cu [15, 19], Ru [20], Ir [21] and Pt [22] have often been used for the synthesis of graphene films. While catalytically-synthesized graphene films have a disadvantage of having to be formed on conductive metal materials, some useful ideas on transfer-free techniques have been suggested [23-30]. Recently, we have also reported that graphene films can be formed directly on insulating SiO_2/Si by using a thin Ni film as an underlying catalyst film [23]. Figure 1 shows explanatory drawings of the graphene synthesis process [23]. First, a Ni/SiO_2/Si stacking structure with the Ni film thinner than 50 nm is prepared as a substrate for graphene synthesis. Then, an amorphous carbon (a-C) film is deposited on the Ni film, where we use the pulse arc plasma deposition (PAPD) technique [17]. Then, the graphene film is formed via the dissolution and precipitation at a high temperature, and at almost the same time, spontaneous agglomeration of the Ni metal occurs. It was speculated that the nucleation of graphene preferentially starts from the step sites on the granulating Ni films [9, 17, 23]. Kato and Hatakeyama have reported that graphene nano-ribbons can be grown from Ni nano-bars [31], which is considered to be due to a phenomenon similar to our process. As a result, the graphene film is grown directly on the SiO_2 film. Although island-shaped metallic particles remain on the surface, it was confirmed that they can easily be removed by dipping in a hydrochloric acid [23]. This process seems similar to that reported by Kwak et

al [25], who have proposed a low-temperature transfer-free graphene synthesis process utilizing the carbon diffusion through microstructured Ni films. In this case, the initial carbon deposition must be preceded by the formation of the Ni microstructure. Contrarily, our process causes the graphene precipitation and metal agglomeration at almost the same time during a single thermal treatment. We believe that this process can expand the possibility of graphene synthesis technique utilizing catalytic reactions. To continue further development on the process, however, more detailed study is indispensable especially as to how the graphene films are formed and two-dimensionally distributed on the surfaces. In this paper, therefore, we attempted comprehensive study on our graphene synthesis process. Thin Co films were also examined as a catalytic metal in addition to Ni films. The dependency on annealing temperatures as well as on metal film thicknesses was carefully investigated. The multipoint Raman mapping technique was employed to analyze how the graphene films are formed and two-dimensionally distributed on the surfaces.

2. EXPERIMENTAL

Ni/SiO_2/Si and Co/SiO_2/Si stacking structures with different metal film thicknesses of 10, 20 and 30 nm were used as starting substrates for graphene synthesis, where the thin Ni and Co films were deposited on 100-nm-thick SiO_2 films on Si (111) substrates by electron-beam (EB) evaporation. The a-C films were deposited in an ultrahigh-vacuum PAPD chamber [17, 23], in which the discharge pulse number was maintained at 50 pulses. Subsequently, the samples were annealed at different temperatures of 700°C, 800°C, 900°C and 1000°C for 5 min in nitrogen gas flow ambient. After the annealing processes, sample surfaces were observed by scanning electron microscope (SEM). In order to observe the cross-sectional nanostructure, the transmission electron microscope (TEM) study including high-resolution TEM (HR-

TEM) and scanning TEM (STEM) was carried out. In the STEM observation, the high-angle annular-dark-field (HAADF) observation and energy-dispersive X-ray spectroscopy (EDS) were applied in addition to the conventional bright-filed (BF) observation. The EDS point analyses were conducted with an electron-beam spot size of less than 1 nm. For the cross-sectional TEM observation, samples were thinned to the thickness of approximately 80 nm with the use of a focus ion beam system (SMI3050TB), in which a Ga^+ ion was used as the ion beam source by accelerating to an energy of 30 keV. To investigate how the graphene films were formed and two-dimensionally distributed on the surfaces, the multipoint Raman mapping was carried out, in which a 532-nm-wavelength solid-state laser with the output power of 10 mW was used as an excitation light source. For the Raman mapping study, the spot size of the incident laser and the distance between measured points were maintained at 1 μm and 0.2 μm, respectively, for a scanning area of 5 μm × 5 μm.

3. RESULTS AND DISCUSSION

3.1. Electron microscope study

Figures 2(a) and 2(b) show SEM images for annealed surfaces of samples with the different-thickness metal films of Ni and Co, respectively. It was confirmed that the metal agglomeration occurred on both kinds of samples. In our experiments, significant differences in metal agglomeration have not been observed between samples with and without the carbon layer on top of the metals. From these figures, the size of the island-shaped particles clearly increased with the increase in the metal thicknesses, which is almost consistent with the result of our previous report [23]. Also, the present study provides additional information, which is about the temperature dependency and about the agglomeration of the Co films. From the observation results, the progress of Co agglomeration appeared to be quite similar but

somewhat slower compared to the case of Ni films. This seems to be due to the similarity and small difference in their cohesive energies (102 kcal/mol for Ni and 105 kcal/mol for Co) [32] and melting points (1,728K for Ni and 1,768K for Co) [33]. As for the temperature dependency, it is clear that the metal agglomeration progressed well with the increase in the annealing temperature. Basically, the metal agglomeration originates from the surface migration of metals, which occurs by transforming the heat energy into the kinetic energy for lowering their surface energy. Therefore, it is natural to consider that the thicker metal films did not migrate at a low temperature. For both kinds of the samples, the metal agglomeration was almost completed at temperatures higher than 900°C.

Typical cross-sectional HR-TEM images around the particles are shown in Figures 3(a) and 3(b), which have been taken after annealing at 900°C for samples with the 20-nm-thick Ni and Co films, respectively. Here, the images in Figure 3(a) are the same as shown in our previous report [23]. The dark rounding areas seen in these images correspond to the cross section of an island-shaped particle. From these images, the formation of multilayer graphene is confirmed for both samples, and they appear to be formed directly on SiO_2 films. The observation results showed that the graphene films derived from Co were thicker than those from Ni. We speculate that it was caused by the difference in solid solubility limits at the maximum reaction temperatures and at precipitation temperatures. Samples were then evaluated by STEM including HAADF and EDS analyses, and the results are summarized in Figures 4(a) and 4(b), where the EDS analyses were taken by focusing on cross sections of particles (positions A and E), graphene films (positions B and F), graphene/SiO_2 boundaries (positions C and G) and SiO_2 films (positions s D and H), respectively. The results revealed that particles consisted mainly of metallic atoms, and that graphene films were directly on SiO_2 films. In Figure 4(a), a small amount of Pd is observed inside the metallic particle, which is probably a result of contamination incorporated from our EB

evaporation furnace. On the basis of the above, the thin Ni and Co films proved to be equally useful for this transfer-free graphene-synthesis process. On the other hand, metallic particles appeared to be penetrating onto SiO_2 surfaces, as seen in Figures 3 and Figure 4. This indicates that the catalyst metals reacted with SiO_2 in the process of metal agglomeration. The EDS results support this idea, which show that the metallic particles contain a certain amount of Si. The uneven SiO_2 surface as observed in Figure 3 or Figure 4 is probably another evidence of the reaction.

3.2. Microscopic Raman Study

A few examples of Raman mapping results are shown in Figure 5, in which the views of optical microscopic (OM) images are almost consistent to those of the Raman mapping images. Although the OM images are not as clear as SEM images as seen in Figure 2, it is possible to recognize their morphology changes by comparing with the SEM images. The Raman intensity maps represent the two-dimensional distributions of the relative integrated intensities of 2D band (2,700 cm^{-1}), which confirms the existence of graphene films. Figure 5(a) shows a surface after annealing at 700°C for a sample with the Ni thickness of 30 nm. As for this sample, there seemed to be almost no graphene films on Ni-remained areas, but they obviously existed around specific areas uncovered with Ni metals. This indicates that graphene films were preferentially synthesized at areas where Ni films disappeared with the progress of agglomeration. This phenomenon does not contradict the information that the graphene nucleation preferentially starts from the step sites on metal surfaces [9, 17, 23]. Figures 5(b) and 5(c) show surfaces after annealing at 900°C for samples with the 20-nm-thick Ni films and Co films, respectively, which are the same samples as shown in Figure 3 and Figure 4. For these samples, graphene films almost completely covered the whole observation surfaces, which even includes areas showing the weakest

Raman signals. Note that this estimation is limited within the spatial resolution of this observation technique, which approximately corresponds to the incident-laser spot size of 1 μm. From this observation, however, neither huge pinholes nor clearly divided pieces were observed on both kinds of samples despite the existence of many metallic particles on their surfaces. This will be accepted as a positive indication considering future perspective of this graphene synthesis process.

To achieve further understanding for the graphene formation processes as well as for their two-dimensional distributions on the surfaces, the Raman mapping data were statistically treated. Figure 6(a) shows the changes in the integrated Raman intensity ratio of the G band (1,590 cm^{-1}) to the 2D band (I_G/I_{2D} ratio), which are considered to be related to the layer number in graphene films [34]. Further, Figures 6(b) and 6(c) show the changes in the ratio of the D band (1,350 cm^{-1}) to the G band (I_D/I_G ratio), and the changes in the full-width at half maximums of 2D peaks (2D-FWHMs), respectively, which are considered to represent structural disorders of graphene films [34]. Here, each of the data was taken from almost completely metal-agglomerated samples. All of the figures plot the average values obtained from the multipoint Raman measurements as seen in Figure 5, and the standard deviation (σ) changes of the I_G/I_{2D} ratio, I_D/I_G ratio and 2D-FWHMs are also plotted in the same figures. As shown in these figures, it was found that the changes in the Raman signals depend strongly not on the annealing temperatures but rather on the starting metal thicknesses, which was observed for both kinds of metals. Furthermore, the evaluated Raman parameters showed a tendency of having lower values with the increase in metal thicknesses. This indicates that graphene films derived from thicker metal films have better structural qualities with lower layer numbers. Generally, the graphene synthesis process utilizing catalytic reaction is explained by the phenomenon that carbon atoms alloyed with catalyst metals precipitate out as graphene during cooling processes in accordance with the solubility limit. Therefore, it seems understandable that

the larger amount of graphene is precipitated out from the thinner metal films due to their incorporation limit. As for the quality of graphene films, it can be speculated that the increase in the layer number caused the structural disorder of graphene films. This indicates that the layer number as well as the film quality can be controlled over by choosing the appropriate metal thickness and carbon deposition amount. In addition, the standard deviation data indicates that the synthesized graphene films showed relatively good two-dimensional uniformities at almost all stages. This is also considered a positive indication for future research of this graphene synthesis process.

4. SUMMARY AND CONCLUSIONS

In summary, we investigated the transfer-free graphene synthesis process utilizing metal agglomeration phenomena. The SEM and TEM study indicated that multilayer graphene was synthesized on SiO_2 films as a consequence of metal agglomeration, which was equally observed on Ni and Co catalyst films. The microscopic Raman mapping study indicated that graphene films were preferentially synthesized at areas where metal films disappeared at an early stage of their agglomeration, and that they finally covered almost the whole surfaces. The synthesized graphene films showed a tendency of having better structural qualities and lower layer numbers with the increase in the metal thicknesses. Also, they showed relatively good two-dimensional uniformities at almost all stages, as long as the metal agglomeration sufficiently progressed. We believe that the present results will provide useful information to future perspective of the graphene synthesis process utilizing catalytic reaction.

[1] Novoselov K S, Geim A K, Morozov S V, Jiang D, Zhang Y, Dubonos S V, Grigorieva I V and Firsov A A 2004 *Science* **306** 666–669

[2] Wu Y H, Yu T and X Shen Z, 2010 *J. Appl. Phys.* **108** 071301-1–38

[3] Lin Y M, Dimitrakopoulos C, Tenkins K A, Farmer D B, Chiu H Y, Grill A and Avouris Ph 2012 *Science* **327** 662–662

[4] Schwierz F 2010 *Nat. Nanotechnol.* **5**487–496

[5] Forbeaux I, Themlin J M and Debever J M 1998 *Phys. Rev.* B **58** 16396–16406

[6] Emtsev K V, Bostwick A, Horn K, Jobst J, Kellogg G L, Ley L, McChesney J L, Ohta T, Reshanov S A, R€ohrl J, Rotenberg E, Schmid A K, Waldmann D, Weber H B and Seyller T 2009 *Nat. Mater.* **8** 203–207

[7] Suemitsu M and Fukidome H 2010 *J. Phys. D: Appl. Phys.* **43** 374012-1–11

[8] Ouerghi A, Kahouli A, Lucot D, Portail M, Travers L, Gierak J, Penuelas J, Jegou P, Shukla A, Chassagne T and Zielinski M 2010 *Appl. Phys. Lett.* **96** 191910-1–3

[9] Reina A, Jia X, Ho J, Nezich D, Son H, Blovic V, Dresselhaus M S and Kong J 2009 *Nano Lett.* **9** 30–35

[10] Kim E, Lee W G and Jung J 2011 *Electron. Mater. Lett.* **7** 261–264

[11] Miyata Y, Kamon K, Ohashi K, Kitaura R, Yoshimura M and Shinohara H 2010 *Appl. Phys. Lett.* **96** 263105-1–3

[12] Zheng M, Takei K, Hsia B, Fang H, Zhang X, Ferralis N, Ko H, Chueh Yu L, Zhang Y, Maboudian R and Javey A 2010 *Appl. Phys. Lett.* **96** 063110-1–3

[13] Kim K S, Zhao Y, Jang H, Lee S Y, Kim J M, Kim K S, Ahn J, Kim P, Choi J and Hong B H 2009 *Nature* **457** 706–710

[14] Kim Y, Song W, Lee S Y, Jeon C, Jung W, Kim M and Park C-Y 2011 *Appl. Phys. Lett.* **98** 263106-1–3

[15] Kim J, Ishihara M, Koga Y, Tsugawa K, Hasegawa M and Iijima S 2011 *Appl. Phys. Lett.* **98** 091502-1–3

[16] Keidar M, Shashurin A, Li J, Volotskova O, Kundrapu M and Zhuang T S 2011 *J. Phys. D: Appl. Phys.* **44** 174006-1–6

[17] Fujita K, Banno K, Aryal H R and Egawa T 2012 *Appl. Phys. Lett.* **101** 163109-1–3

[18] Yu Q, Lian J, Siriponglert S, Li H, Chen Y P and Pei S 2008 *Appl. Phys. Lett.* **93** 113103-1–3

[19] Li X, Cai W, An J, Kim S, Nah J, Yang D, Piner R, Velamakanni A, Jung I, Tutuc E, Banerjee S K, Colombo L and Ruoff R S 2009 *Science* **324** 1312–1314

[20] Sutter P W, Flege J I and Sutter E A 2008 *Nat. Mater.* **7** 406–411

[21] Coraux J, N'Diaye A T, Busse C and Michely T 2008 *Nano Lett.* **8** 565–570

[22] Ono R, Hosoda M, Okuzawa M, Tagawa M, Oshima C and Otani S 2000 *Tanso* **195** 400–404

[23] Banno K, Mizuno M, Fujita K, Kubo T, Miyoshi M, Egawa T and Soga T 2013 *Appl. Phys. Lett.* **103** 082112-1–4

[24] Yan Z, Peng Z, Sun Z, Yao J, Zhu Y, Liu Z, Ajayan P M and Tour J M 2011 *ACS nano* **5** 8187–8192

[25] Kwak J, Chu J H, Choi J, Park S, Go H, Kim S Y, Park K, Kim S, Kim Y, Yoon E, Kodambaka S and Kwon S 2012 *Nat. Commun.* **3** 645-1–7

[26] Pan G, Li B, Heath M, Horsell D, Wears M L, Taan L A and Awan S 2013 Carbon **65** 349–358

[27] Kim W, Debnath P C, Lee J, Lee J H, Lim D and Song Y 2013 *Nanotechnol.* **24** 365603-1–7

[28] Gumi K, Ohno Y, Maehashi K, Inoue K and Matsumoto K 2012 *Jpn. J. Appl. Phys.* **51** 06FD12-1–4

[29] Kondo D, Sato S, Yagi K, Harada N, Sato M, Nihei M and Yokoyama N 2010 *Appl. Phys. Express* **3** 025102-1–3

[30] Kato T and Hatakeyama R 2012 *ACS nano* **6** 8508–8515

[31] Kato T and Hatakeyama R 2012 *Nat Nanotechnol.* **7** 651–656

[32] Griffith J S 1956 *J. Inorg. Nucl. Chem* **3** 15–23

[33] Dinsdale A T 1991 *CALPHAD* **15** 317−425

[34] Graf D, Molitor F, Ensslin K, Stampfer C, Jungen A, Hierold C and Wirtz L, 2007 *Nano Lett.* **7** 238–242

Figure captions

Figure 1. (Color online) Schematic drawings for the graphene synthesis process utilizing the metal agglomeration phenomena; (a) Amorphous carbon film is deposited on Ni/SiO_2/Si substrate. (b) After annealing, graphene films are formed on the SiO_2 film with metallic particles. (c) Metallic particles are removed by dipping in a hydrochloric acid solution.

Figure 2. Surface SEM images for after annealing samples with different-thickness (a) Ni and (b) Co films. The scale bars are 1 μm.

Figure 3. Cross-sectional TEM images and its magnified HR-TEM images after annealing at 900°C for samples with 20-nm-thick (a) Ni films and (b) Co films, in which the dark rounded area corresponds to cross sections of island-shaped particles.

Figure 4. Cross-sectional BF-STEM and HAADF-STEM images after annealing at 900°C for samples with 20-nm-thickness (a) Ni and (b) Co films. Tables show results of EDS analyses taken from specific points marked in HAADF-STEM images.

Figure 5. (Color online) Integrated Raman intensity maps for 2D bands with OM view images, and Raman spectra from a few specific points in the Raman maps. Samples are (a) 30-nm-thick Ni films annealed at 700°C and (b) 20-nm-thick Ni films annealed at 900°C, and (c) 20-nm-thick Co films annealed at 900°C. In Raman maps, the increase in the intensities corresponds to the change in color from dark blue to red.

Figure 6. Metal thickness dependence of (a) I_G/I_{2D} ratio, (b) I_D/I_G ratio and (c) 2D-FWHMs, in which the standard deviation values (σ) of those are also shown. All of the data were taken from the microscopic Raman mapping measurements as seen in Fig. 5.

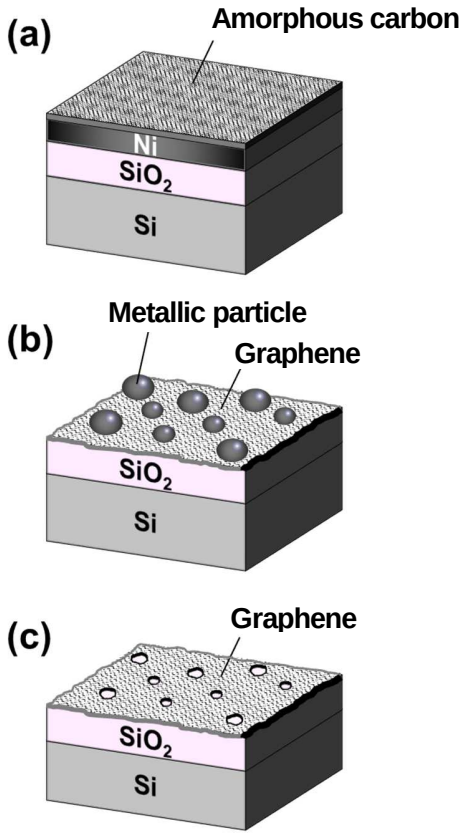

Figure 1 Miyoshi et al.

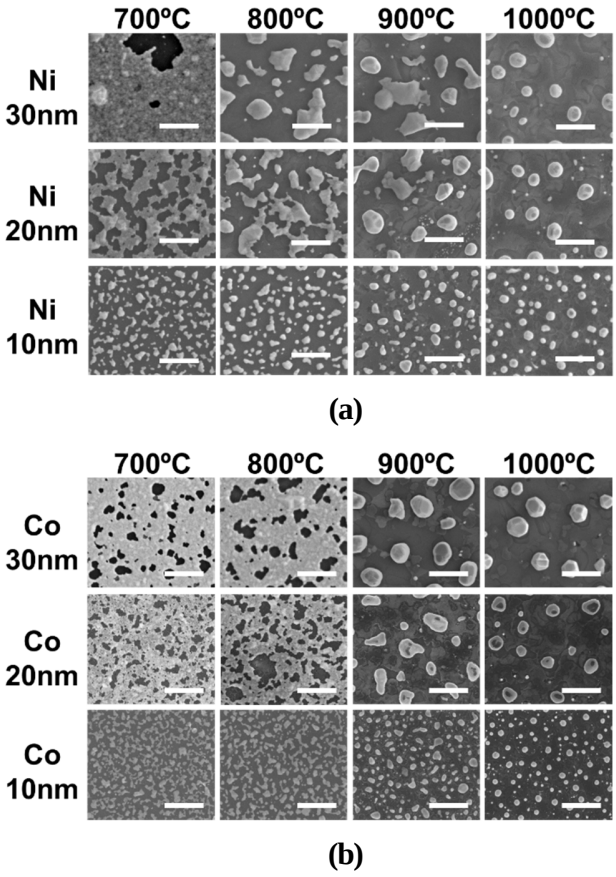

Figure 2 Miyoshi et al.

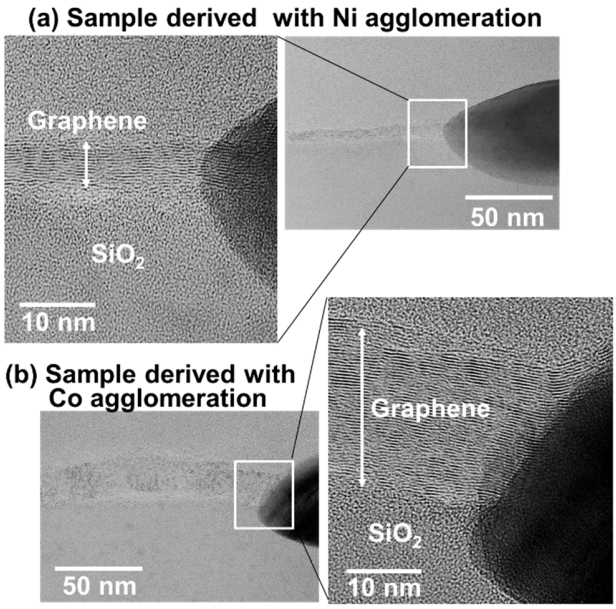

Figure 3 Miyoshi et al.

(a) Sample derived with Ni agglomeration

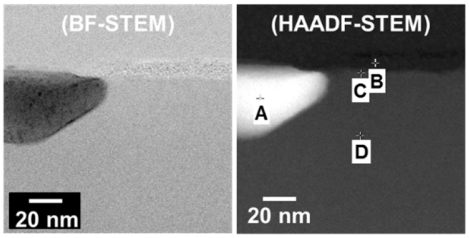

Position	C	O	Si	Ni	Pd	Total
A.	16.0	26.1	19.1	36.8	1.9	100.0
B.	99.5	0.0	0.5	0.0	0.0	100.0
C.	26.3	42.5	31.2	0.0	0.0	100.0
D.	0.0	57.9	42.1	0.0	0.0	100.0

(atm.%)

(b) Sample derived with Co agglomeration

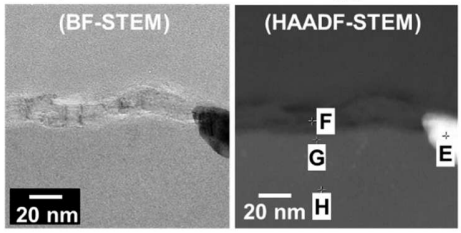

Position	C	O	Si	Co	Total
E.	26.8	3.8	12.1	57.3	100.0
F.	98.8	0.6	0.6	0.0	100.0
G.	13.6	51.3	35.1	0.0	100.0
H.	0.9	60.9	38.2	0.0	100.0

(atm.%)

Figure 4 Miyoshi et al.

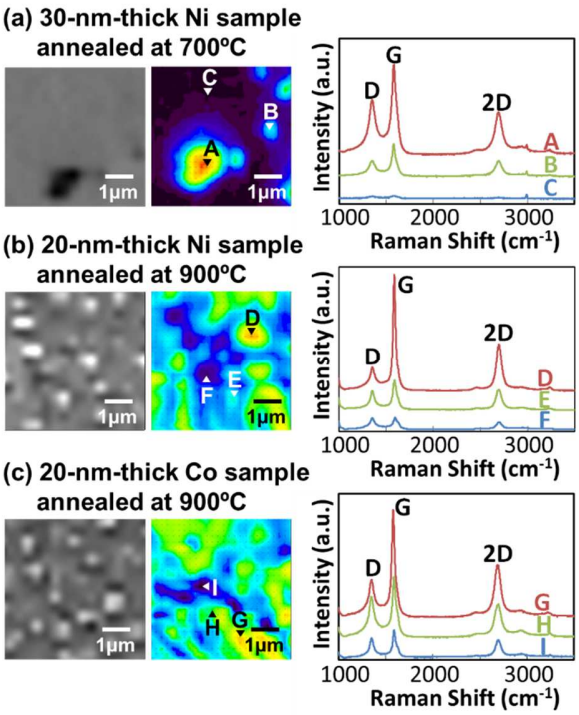

Figure 5 Miyoshi et al.

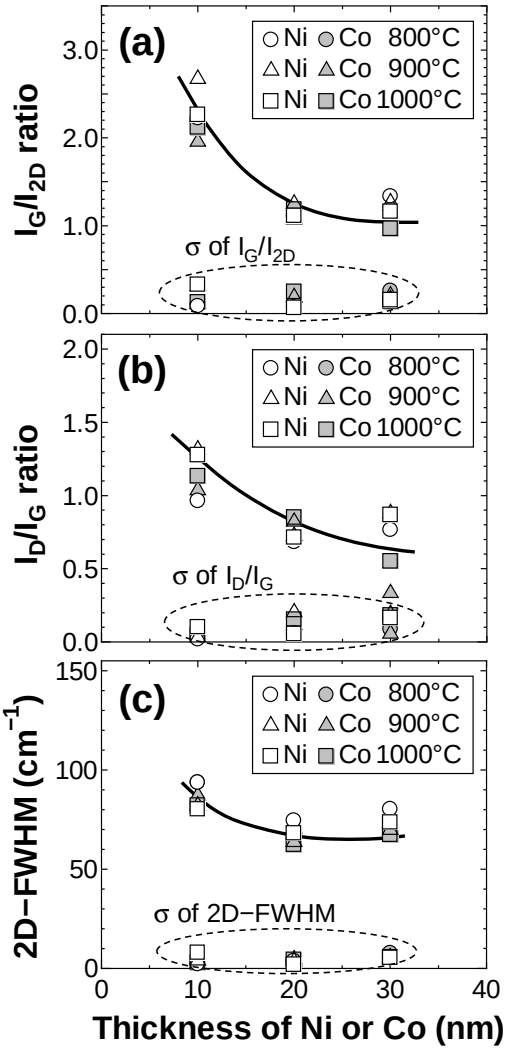

Figure 6 Miyoshi et al.